

GazeHTA: End-to-end Gaze Target Detection with Head-Target Association

Zhi-Yi Lin¹ Jounh Yeong Chew² Jan van Gemert¹ Xucong Zhang¹
¹Computer Vision Lab, Delft University of Technology
²Honda Research Institute Japan

Abstract. We propose an end-to-end approach for gaze target detection: predicting a head-target connection between individuals and the target image regions they are looking at. Most of the existing methods use independent components such as off-the-shelf head detectors or have problems in establishing associations between heads and gaze targets. In contrast, we investigate an end-to-end multi-person **G**aze target detection framework with **H**eads and **T**argets **A**ssociation (*GazeHTA*), which predicts multiple head-target instances based solely on input scene image. GazeHTA addresses challenges in gaze target detection by (1) leveraging a pre-trained diffusion model to extract scene features for rich semantic understanding, (2) re-injecting a head feature to enhance the head priors for improved head understanding, and (3) learning a connection map as the explicit visual associations between heads and gaze targets. Our extensive experimental results demonstrate that GazeHTA outperforms state-of-the-art gaze target detection methods and two adapted diffusion-based baselines on two standard datasets.

1 Introduction

Human attention estimation using visual observations is critical for real-world applications such as human-robot interaction [1, 30, 32], social activity recognition [12], mental health diagnosis [3], and customer behavior analysis [38]. The common solution for human attention estimation is to infer the 3D direction of gaze from human eyes [45, 46] or face [7, 46]. However, many downstream applications require the specific region or object that a person is looking at, i.e., the gaze target, rather than the gaze direction.

Gaze target detection aims to directly associate individuals and their gaze targets within a single image [25] or across multiple video frames [26], offering an end-to-end solution for human attention estimation. Most of the gaze target detection approaches employ two-stream architectures, where one stream focuses on scene feature extraction while the other one learns head features [2, 8, 9, 16]. These approaches face challenges such as the lack of direct association between heads and gaze targets, and the dependency on off-the-shelf head detectors as demonstrated in recent studies [40, 41]. Moreover, the majority of previous methods are restricted to processing one head at a time, requiring repeated processing to identify gaze targets for all individuals in the scene when multiple people are present. The work of Tu et al. [41] addresses the challenges in the two-stream

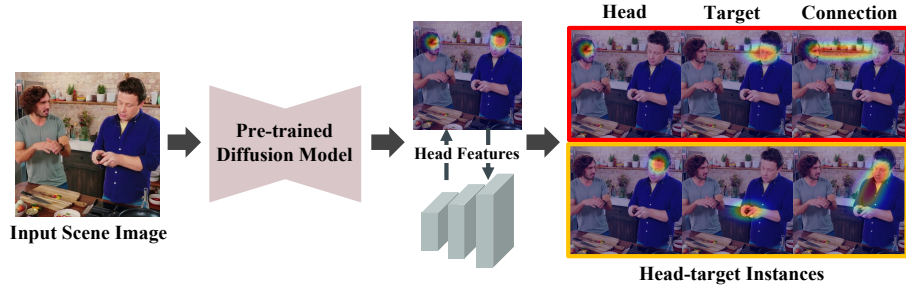


Fig. 1: Overview of GazeHTA, which takes the scene image as input to predict head-target instances. GazeHTA consists of a pre-trained diffusion model as the scene feature extractor, a head feature re-injection mechanism, and the connection maps as the visual associations between heads and gaze targets.

approaches with an end-to-end multi-person gaze target detection method, to directly predict multiple pairs of head-target instances. Nevertheless, this approach does not establish strong connections between heads and gaze targets, which restricts the final detection accuracy. The work of Tonini et al. [40] improves the association between heads and gaze targets, and achieves state-of-the-art performance. It is, however, not fully end-to-end due to its dependency on preliminary object detection. Pre-training the object detector also limits the object categories considered for gaze targets. This constraint may exclude diverse object classes or regions within the environment that are beyond the scope of the pre-trained object detector.

Thus, there are two major challenges in gaze target detection: 1) detecting the heads and the gaze targets; and 2) associating heads and gaze targets to predict which head is looking at which target. Addressing the first challenge involves identifying the relevant heads, objects or other regions as potential gaze targets. This can be addressed using powerful feature extractors, such as diffusion-based models, which have demonstrated remarkable performance in various visual perception tasks [6, 14, 27, 29, 47]. However, effectively integrating these pre-trained large foundation models into gaze target detection remains an open question. The second challenge entails linking heads and gaze targets, which requires gaze target localization while considering the presence of individual heads. Despite efforts to employ gaze estimation results as constraints on the gaze target locations [13, 16, 35, 40], most existing methods have not fully addressed the association between heads and gaze targets.

In this paper, we propose GazeHTA: a novel end-to-end framework for multi-person gaze target detection from a single scene image. We exploit features from a pre-trained diffusion model, while emphasizing head and facial regions with a novel re-injection method. We then associate the heads and gaze targets explicitly by a connection map in the image. These connection maps serve as links between the heads and gaze targets in the image, offering additional supervision

during model training. An overview is shown in Fig. 1. Our experiments demonstrate that GazeHTA achieves state-of-the-art performance while not being restricted to the diffusion model backbone. In summary, the main contributions of this paper include:

- We are the first to exploit the rich semantic features from the pre-trained diffusion model for the gaze target detection task.
- We propose a head feature re-injection to improve the head priors, and a connection map to explicitly associate heads and gaze targets.
- Our extensive experiments show the proposed GazeHTA achieves state-of-the-art performances on standard datasets.

2 Related Works

2.1 Gaze Target Detection

Formulated by [25], gaze target detection is to determine the location where a person is looking within a scene image, or across video frames [26]. A two-stream approach is a common strategy with one stream focusing on scene understanding, while another one learning head features from input head crops, detected by an off-the-shelf head detector [8, 9, 16, 36]. Various modalities such as temporal information [9], depth [2, 13, 35, 39], and 2D pose [2] have been incorporated to increase accuracy. However, relying on off-the-shelf models for head crops or incorporating multiple modalities remains challenging, particularly in ensuring model robustness for real-world scenarios. Studies have shown a significant performance drop when the input head crops are detected by off-the-shelf detectors instead of human annotations [40, 41].

Recently, end-to-end approaches have emerged to simultaneously detect multiple heads and their associated gaze targets [40, 41]. The HGTTR is a transformer-based network that predicts several head-target instances comprising head locations, out-of-frame flags, and gaze heatmaps [41]. Unfortunately, its performance suffers from brittle associations between heads and gaze targets. As a result, the latest advancements in multi-person gaze target detection have led to the development of object-aware frameworks, which leverage the concept of objects to establish associations between heads and gaze targets [40, 42]. The object-aware frameworks initially predict objects and subsequently associate head objects with all detected objects for gaze target detection. However, these methods revert to a two-stage approach because of their reliance on detected objects for head-object association. Moreover, the scope of gaze targets is limited to a subset of classes for which the pre-trained object detector was trained, raising concerns about the robustness and applicability of these methods in real-world scenarios. In contrast to previous approaches, GazeHTA offers an end-to-end solution with implicit target feature extraction, enhanced head priors, and finally, an explicit association between heads and gaze targets through connection maps.

2.2 Diffusion Models

Originally from diffusion probabilistic models [34], diffusion models are generative models designed to learn the distribution of data for generating new samples resembling the training data. This process involves iteratively applying a series of transformations from a noise image to a realistic image [23, 27, 28]. A significant milestone in text-to-image generation has been achieved by Stable Diffusion [27] and DALL-E [24]. In particular, Stable Diffusion is released with open-source code and operates within the latent space of powerful pre-trained autoencoders, enabling training on limited computational resources while preserving quality and flexibility.

With the remarkable success of diffusion models in image generation, recent studies showed their potential across various downstream visual perception tasks [10, 37]. It is straightforward to integrate a pre-trained diffusion model within diffusion-based pipelines, where target outputs are generated by iteratively removing noise from input noise sources [6, 14, 20, 31]. This strategy can be extended to gaze target detection, where the scene image serves as the condition for predicting head and gaze heatmaps through multi-step denoising. However, text-to-image diffusion models are primarily designed to generate high-quality images from noise, while our gaze target detection task uses connection map prediction. Therefore, directly applying the denoising process may not be efficient for gaze target detection.

Alternatively, pre-trained diffusion models can be used as feature extraction backbones, without engaging in the progressive denoising process [5, 47]. Despite its simplicity, employing a pre-trained diffusion model as a feature extractor is effective for various visual perception tasks, including image segmentation and depth estimation [43, 47]. Considering the output format of gaze target detection is a heatmap which resembles that of image segmentation and depth estimation, namely the spatial maps or heatmaps, they may potentially benefit from the same model architecture. Following the same strategy, GazeHTA employs a pre-trained diffusion model as the backbone to extract both high-level and low-level semantic features for object understanding and head localization, which are crucial for accurate gaze target detection.

3 GazeHTA

The pipeline of GazeHTA is shown in Fig. 2. Taking only a scene image as the input, GazeHTA extracts multi-scale scene features for out-of-frame binary predictions and head-target proposals. For the head-target proposal, a head feature is learned and re-injected back to enhance the head priors. Subsequently, heads, gaze targets, and connection maps are predicted in the form of heatmaps. Within each head-target instance, GazeHTA establishes a visual association between the head and its corresponding gaze target by a connection map.

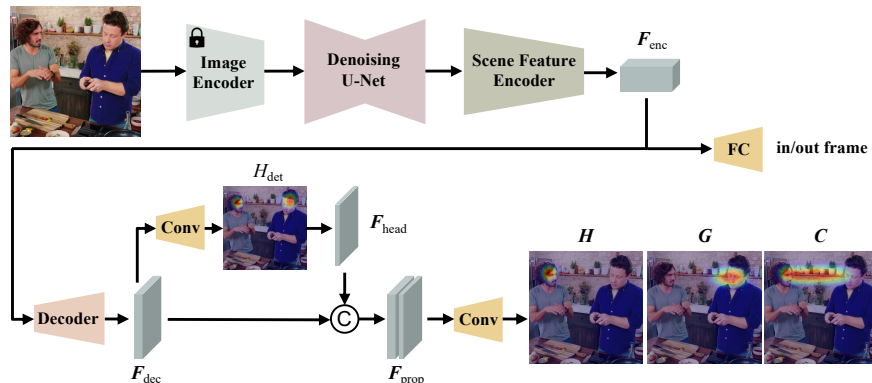


Fig. 2: Network architecture of GazeHTA. The input scene image is transformed into scene features through a pre-trained image encoder and a denoising U-Net. The scene features are encoded into F_{enc} for out-of-frame predictions via a fully connected layer (FC), and for head-target proposals. In the head-target prediction branch, a learned head feature F_{head} is re-injected and fused with the decoded feature F_{dec} . The resulting feature F_{prop} is then used to predict N head-target proposals, including head heatmaps H , gaze heatmaps G , and connection maps C , which are explicitly learned to associate the head and gaze target. Conv represents convolutional layers.

3.1 Scene Feature Extraction

In GazeHTA, the backbone to extract scene features is a pre-trained denoising U-Net from Stable Diffusion [27]. The use of Stable Diffusion, a large-scale text-to-image generator, is due to its capability to encompass features with both low-level and high-level semantic knowledge [22] acquired from large-scale real-world data. By taking the scene image as the only input, GazeHTA encodes it with a pre-trained image encoder, followed by a denoising U-Net from the pre-trained diffusion model. We extract intermediate features from four different levels in the U-Net with a similar operation to the VPD method [47]. These multi-scale scene features are then encoded into a compact representation, denoted as $F_{enc} \in \mathbb{R}^{3520 \times 16 \times 16}$. F_{enc} is utilized for both out-of-frame predictions and head-target proposals. We expect the implicit understanding of the scene features can facilitate the identification of potential heads and gaze targets.

Note that, unlike VPD [47], we eliminate the entire text prompt module by removing the cross-attention layers in the denoising U-Net, as it is not necessary nor effective for the gaze target detection task.

3.2 Head Feature Re-injection

Accurately locating the human head position is essential for successful gaze target detection. To improve head detection, we introduce supervision on a head detection map, which aims to detect all instances of heads within the scene image. To this end, the encoded feature F_{enc} is passed through a convolution-based

decoder that gradually expands the spatial dimension of \mathbf{F}_{enc} into a decoded feature, denoted as $\mathbf{F}_{\text{dec}} \in \mathbb{R}^{192 \times 64 \times 64}$. \mathbf{F}_{dec} is then passed through convolutional layers to generate an intermediate head detection map H_{det} for head prior enhancement. To supervise the training on H_{det} , we apply the detection results from the RetinaFace [11] as pseudo labels since the heads are not fully annotated in the training data. Although H_{det} provides insights into potential head positions, we only use it as a soft guidance for later head-target prediction. To this end, we utilize the head priors encoded in its subsequent head feature \mathbf{F}_{head} , which is derived by passing H_{det} through a single convolutional layer. After obtaining head priors, \mathbf{F}_{head} is re-injected and fused with \mathbf{F}_{dec} via concatenation to provide additional guidance for head localization. The resulting feature, denoted as $\mathbf{F}_{\text{prop}} \in \mathbb{R}^{193 \times 64 \times 64}$ is then utilized to predict N head-target proposals.

3.3 Visual Association via Connection Maps

Given the scene feature for locating potential heads and targets, we propose a novel visual association scheme via multi-task learning as the model not only predicts heads and targets but also connection maps as heatmaps. Taking \mathbf{F}_{prop} as input, a prediction head with convolutional layers generates N head-target proposals. Each proposal comprises three types of heatmaps: head heatmaps $\mathbf{H} \in \mathbb{R}^{N \times 64 \times 64}$, the corresponding gaze heatmaps $\mathbf{G} \in \mathbb{R}^{N \times 64 \times 64}$, and the connection maps $\mathbf{C} \in \mathbb{R}^{N \times 64 \times 64}$. In contrast to previous approaches that typically link heads and gaze targets through a gaze vector prediction or the predefined field of view parameters [13, 16, 35, 40], the proposed connection maps \mathbf{C} explicitly learn the link between the heads and targets. This is motivated by the fact that the prediction of head heatmaps \mathbf{H} and gaze heatmaps \mathbf{G} are isolated, so it is essential to have these connection maps \mathbf{C} to force the model to learn their associations. It is important to note that the connection maps \mathbf{C} are a unidirectional mapping that only focus on highlighting the connection between the head and its corresponding target. Through the use of three-heatmap prediction structure, the model is encouraged to learn the individual features of heads and gaze targets, as well as their associations.

3.4 Out-of-frame Flag

Similar to previous gaze target detection works [35, 40, 41], GazeHTA predicts an out-of-frame flag to indicate whether the person is looking outside the frame, in which case the predicted gaze targets are not considered. Same as the head-target proposals, the network utilizes \mathbf{F}_{enc} to predict N out-of-frame flags, denoted as $O \in \mathbb{R}^N$, using a convolutional layer followed by a single fully-connected layer. Although we can use the feature from a later stage, we empirically found that using \mathbf{F}_{enc} for the out-of-frame prediction yields the best overall performance in the final head-target instance prediction. This suggests that out-of-frame prediction may offer early guidance, thereby enhancing the accuracy of head-target proposals. Additionally, this design feature offers practical benefits as it enables

the network to skip the computation of head-target proposals during inference if the predicted gaze target is out-of-frame.

3.5 Training Objective

Bipartite matching is first performed to find the optimal matching between the predicted head-target instances and the ground-truth instances. The loss is then computed between the matched instance pairs.

Bipartite matching. Following the training procedure of [4, 40, 41], we use the Hungarian algorithm [15] for the bipartite matching between the predicted head-target instances and the ground-truth. The bipartite matching finds the best one-to-one matching by minimizing the total matching cost between each ground-truth instance and the candidate predicted head-target instance. The computation of the matching cost for each potential pairing entails a weighted combination of the L2-norm of the gaze heatmaps \mathbf{G} , the head heatmaps \mathbf{H} , along with the L1-norm of the out-of-frame flags O . The weights for bipartite matching of \mathbf{G} , \mathbf{H} , and O are empirically set to 1.0, 2.5, and 1.0, respectively.

Loss function. The total loss is computed using the matched pairs of predicted and ground-truth instances, and is expressed as follows:

$$\mathcal{L}_{total} = \lambda_h \cdot \mathcal{L}_h + \lambda_g \cdot \mathcal{L}_g + \lambda_c \cdot \mathcal{L}_c + \lambda_o \cdot \mathcal{L}_o + \lambda_{det} \cdot \mathcal{L}_{det}, \quad (1)$$

where \mathcal{L}_h , \mathcal{L}_g , and \mathcal{L}_c are losses of head heatmaps, gaze heatmaps, and connection maps. \mathcal{L}_{det} is the loss of head detection maps, and \mathcal{L}_o is the loss of out-of-frame flags. λ_h , λ_g , λ_c , λ_o , and λ_{det} denotes the weights for each loss term.

For the head heatmap loss, we calculate the pixel-wise Mean Squared Error (MSE) between the predicted head heatmap $\{h_1, h_2, \dots, h_M\} \in \mathbf{H}$ and the ground-truth $\mathbf{H}^{gt} = \{h_1^{gt}, h_2^{gt}, \dots, h_M^{gt}\}$ as:

$$\mathcal{L}_h = \frac{1}{M} \frac{1}{mn} \sum_{k=1}^M \sum_{i=1}^m \sum_{j=1}^n [h_k^{gt}(i, j) - h_k(i, j)]^2, \quad (2)$$

where M is the number of ground-truth head-target instances in the input image, m and n are heatmap width and height, and $h_k(i, j)$ is the pixel value of the k -th head heatmap at location (i, j) . The calculation of the MSE loss for \mathcal{L}_g and \mathcal{L}_c are the same as \mathcal{L}_h with corresponding heatmaps.

We also employ MSE loss for the head detection map \mathcal{L}_{det} . Since there is just one head detection map per scene image, the calculation becomes:

$$\mathcal{L}_{det} = \frac{1}{mn} \sum_{i=1}^m \sum_{j=1}^n [h_{det}^{gt}(i, j) - h_{det}(i, j)]^2. \quad (3)$$

Lastly, the out-of-frame flag loss \mathcal{L}_o is defined as the binary cross-entropy loss between the prediction $\{o_1, o_2, \dots, o_M\} \in O$ and the ground-truth $O^{\text{gt}} = \{o_1^{\text{gt}}, o_2^{\text{gt}}, \dots, o_M^{\text{gt}}\}$. The calculation is:

$$\mathcal{L}_o = -\frac{1}{M} \sum_{k=1}^M [o_k^{\text{gt}} \log(o_k) + (1 - o_k^{\text{gt}}) \log(1 - o_k)]. \quad (4)$$

4 Experiments

4.1 Datasets

GazeFollow [25] is a large-scale dataset consisting of 122,143 images with 130,339 annotations on head-target instances. In total, there are 4,782 images with 44,191 head annotations. The gaze target of each head is annotated by ten individuals. We sample 2697 samples from the training set as the validation set. GazeFollow contains human faces and is collected from several public datasets, such as COCO [17] and Action 40 [44]. There was no participant consent form since the data are from public data.

VideoAttentionTarget [9] is a video-based gaze target dataset. It comprises 71,666 frames from 1,331 clips, with 164,514 annotations on head-target instances. Following the training procedure outlined in [39–41], we adopt a sampling strategy on the training data, where one frame is selected from every five consecutive frames to avoid overfitting. We sampled 5769 samples from the training set for validation purposes. The test set of this dataset consists of 2,771 images with 6,377 annotations on head-target instances that remain unchanged in our experiments. The data contain human faces and were retrieved from YouTube videos covering various sources including live interviews, sitcoms, reality shows, and movie clips. There was no participant consent form since the data are from public data.

4.2 Ground-truth Generation.

The ground-truth annotations from the GazeFollow and VideoAttentionTarget datasets only include head bounding boxes and the 2D positions of their corresponding gaze targets. Similarly, the pseudo labels obtained from RetinaFace [11] only include head bounding boxes. To generate the ground-truth head heatmaps \mathbf{H}^{gt} , gaze heatmaps \mathbf{G}^{gt} , and head detection map $H_{\text{det}}^{\text{gt}}$, we assign values with Gaussian distributions centered at the head bounding box centers and gaze points. For the ground-truth connection maps \mathbf{C}^{gt} , we sample 50 points along the straight line connecting the head-target instance and then generate Gaussian distributions for each point. These Gaussian distributions collectively form connection maps \mathbf{C}^{gt} .

4.3 Implementation Details

We use the pre-trained image encoder and denoising U-Net from Stable Diffusion [27] as the backbone. During training, the denoising U-Net is finetuned with a learning rate set to 0.1 of the base learning rate, while the image encoder is frozen without updating. We utilize AdamW optimizer [18] along with a one-cycle-policy learning rate scheduler [33]. For the GazeFollow dataset, the maximum learning rate is set to $3.2e-5$ with 20 epochs of training. For the VideoAttentionTarget dataset, the maximum learning rate is set to $4e-4$ with 10 epochs of training. The weights for training loss λ_h , λ_g , λ_c , λ_o , λ_{det} are set as 1.0, 2.5, 1.0, 1.0, and 1.0, respectively. The number of head-target proposals N is set to 20 following previous works [39, 41]. The output heatmap width m and height n are both set to 64.

4.4 Evaluation Metrics

Following previous works [9, 25, 40, 41], we use the *Area Under Curve* (AUC) and *gaze point distance* (Dist.) metrics for evaluation. These two metrics are assessed exclusively when the ground-truth gaze targets are labeled as “in-frame”. AUC indicates the confidence level of the predicted gaze target locations with respect to the ground-truths. Gaze point distance measures the Euclidean distance between the predicted gaze points and the ground-truths, and it is normalized by the image size. The predicted gaze points are inferred from the location with the maximum value in the gaze heatmaps \mathbf{G} . For the GazeFollow dataset, both the *average distance* (Avg. Dist.) and *minimum distance* (Min. Dist.) are reported due to multiple annotation instances for each given head.

We employ *mean Average Precision* (mAP) to assess the predicted head-target instances, following the setting in [41]. A head-target instance is regarded as true positive if and only if the Intersection-Over-Union (IOU) ratio between the predicted human head box and ground-truth is greater than 0.5, and the normalized gaze distance is less than 0.15. We perform heatmap thresholding [21] followed by contour finding on \mathbf{H} to extract the head bounding boxes. If gaze targets are labeled as out-of-frame, only the head IOU would be considered.

As for the out-of-frame gaze target instances in the VideoAttentionTarget dataset, we report *Average Precision* (AP) on the out-of-frame flags in our evaluation. This metric does not apply to the GazeFollow dataset since the test set only includes in-frame gaze targets.

4.5 Comparison with State-of-the-Art

The quantitative comparison between previous gaze target detection approaches and GazeHTA on the GazeFollow and VideoAttentionTarget datasets is summarized in Tab. 1. It can be seen from the table that GazeHTA outperforms prior works across all evaluation metrics. In contrast to conventional approaches where the understanding of heads and gaze targets is typically acquired independently before integration [2, 9, 13], GazeHTA provides a more unified solution.

Method	GazeFollow				VideoAttentionTarget			
	AUC↑	Avg. Dist.↓	Min. Dist.↓	mAP↑	AUC↑	Dist.↓	AP↑	mAP↑
VideoAttention [9]	0.921	0.137	0.077	-	0.860	0.134	0.853	-
DAM [13]	0.922	0.124	0.067	-	0.905	0.108	0.896	-
ESNet [2]	0.928	0.122	-	-	0.885	0.120	0.869	-
HGTTR [41]	0.917	0.133	0.069	0.547	0.893	0.137	0.821	0.514
Tonini et al. [40]	0.922	0.072	0.033	0.573	0.923	0.102	0.944	0.607
GazeHTA	0.935	0.062	0.025	0.639	0.951	0.069	0.999	0.762

Table 1: Comparison of GazeHTA to other SOTA gaze target detection methods on the GazeFollow and VideoAttentionTarget datasets in terms of gaze target heatmap AUC, gaze point distances (Avg. Dist., Min. Dist., Dist.), head-target instance mAP, and out-of-frame flag AP. GazeHTA outperforms both SOTA two-stage approaches (first to third rows), and SOTA multi-person end-to-end approaches (fourth to fifth rows) across all evaluation metrics.

The advancements stress the importance of concurrently learning the association between heads and gaze targets. Compared to multi-person end-to-end approaches [40, 41], GazeHTA particularly demonstrates significant improvements on mAP, which is specifically designed for measuring head-target association. This shows the effectiveness in accurately identifying both individuals and their associated gaze targets, further highlighting the superiority of GazeHTA in modeling the nuanced correlation between heads and gaze targets.

It is noteworthy that the VideoAttentionTarget dataset is known for its complexity due to the high number of images containing multiple head-target annotations. This characteristic presents a challenge for accurately modeling interactions between multiple individuals and gaze targets. In contrast, the test set of the GazeFollow dataset only contains one in-frame head-target instance per image. Compared to the current SOTA [40], the improvements achieved by GazeHTA on the VideoAttentionTarget dataset (3% in AUC, 32% in Dist., and 26% in mAP) are relatively higher than those on the GazeFollow dataset (1% in AUC, 14% in Avg. Dist., and 12% in mAP). It explicitly demonstrates the efficiency of the integration of the proposed visual association and head feature re-injection techniques.

4.6 Comparison with Diffusion-based Models

One of the contributions of GazeHTA is its utilization of the foundation model Stable Diffusion [27] for the gaze target detection task. To demonstrate its superiority over naive diffusion-based pipelines, we present a comparative analysis between GazeHTA and two SOTA diffusion-based methods, VPD [47] and DDP [14], both of which are based on Stable Diffusion [27] and designed for visual perception tasks, such as semantic segmentation and depth estimation. The results are shown in Tab. 2.

	Text prompts	GazeFollow				VideoAttentionTarget			
		AUC↑	Avg. Dist.↓	Min. Dist.↓	mAP↑	AUC↑	Dist.↓	AP↑	mAP↑
VPD [47]	Fixed	0.915	0.079	0.038	0.517	0.942	0.082	0.999	0.719
VPD [47]	ClipCap [19]	0.920	0.072	0.032	0.556	0.937	0.076	1.000	0.717
VPD [47]	-	0.927	0.067	0.028	0.572	0.943	0.083	0.999	0.706
DDP [14]	-	0.919	0.077	0.036	0.535	0.932	0.090	0.999	0.685
GazeHTA	-	0.935	0.062	0.025	0.639	0.951	0.069	0.999	0.762

Table 2: Comparison of GazeHTA with SOTA diffusion-based methods, VPD [47] and DDP [14], adapted for the gaze target detection task. All these methods utilize the same pre-trained Stable Diffusion model [27] as the backbone. GazeHTA presents the leading performance among diffusion-based methods for gaze target detection. It shows the efficacy of methodological design with model components.

The first baseline, VPD [47], employs a denoising U-Net to extract multi-scale features. We adapt VPD for gaze target detection by taking the scene image as input and then predicting the head heatmaps, gaze heatmaps, and out-of-frame flags. We evaluate the method with three different text prompt options, including i) a fixed text prompt “human faces looking at faces or objects” applied across all input images, ii) text prompts are generated for each image using an image captioner ClipCap [19], and iii) without text prompts and corresponding cross-attention layers.

The second baseline, DDP [14], is a “noise-to-prediction” conditional generative method. We adapt this framework by utilizing a scene image as the condition to iteratively eliminate noise from the input noise, followed by the prediction of head heatmaps, gaze heatmaps, and out-of-frame flags. In our experiment, we set the number of iterations during evaluation to five. The results are shown in the fourth row of Tab. 2.

By comparing the results in Tab. 2 and Tab. 1, it is evident that VPD and DDP achieve comparable or even better results to previous gaze target detection methods on both GazeFollow and VideoAttentionTarget datasets. This shows the potential of pre-trained diffusion models, trained on large-scale datasets, to generalize effectively to the gaze target detection task. Despite involving a multi-step diffusion process, the DDP implementation does not outperform VPD which only uses U-Net as a feature extractor. This observation suggests that the complex diffusion process may not offer benefits for the gaze target detection task. Based on the VPD method with variant text prompt settings, we argue that the benefit of using text prompts for gaze target detection is not significant and also not necessary. Therefore, we remove the text prompt for the final GazeHTA.

Still, GazeHTA outperforms VPD and DDP on both datasets, clearly demonstrating the efficacy of the methodological design presented in this paper for improving performance in the gaze target detection task.

Backbone	C	F_{head}	GazeFollow				VideoAttentionTarget			
			AUC \uparrow	Avg. Dist. \downarrow	Min. Dist. \downarrow	mAP \uparrow	AUC \uparrow	Dist. \downarrow	AP \uparrow	mAP \uparrow
Stable Diffusion [27]	\times	\times	0.927	0.067	0.028	0.572	0.944	0.081	0.998	0.759
	\checkmark	\times	0.927	0.068	0.030	0.606	0.946	0.071	1.000	0.751
	\checkmark	\checkmark	0.935	0.062	0.025	0.639	0.951	0.069	0.999	0.762
DETR [4]	\checkmark	\checkmark	0.928	0.064	0.028	0.607	0.938	0.080	1.000	0.678

Table 3: Ablation study on model components and backbones. We evaluate the two model components, including head feature re-injection (denoted as F_{head}) and connection maps (denoted as C) to show their effectiveness on two datasets. We switch the backbone from Stable Diffusion to DETR to demonstrate that the model components are not restricted to the diffusion model backbone.

4.7 Ablation Study

Model components. We further investigate the incremental effectiveness of individual model components within GazeHTA, namely the head feature re-injection and the connection map. The results of this ablation study are presented in the first three rows of Tab. 3, with the third row showing the performance of our complete model GazeHTA. Note that the baseline model without the head feature re-injection nor the connection map is in the first row, which is essentially the VPD [47] without text prompt in Tab. 2.

We consistently observe improvements in both average gaze point distances and mAP over the baseline when incorporating both the connection map and head feature re-injection. On the GazeFollow dataset, we observe improvements of 7% (0.062 vs. 0.067) in Avg. Dist. and 12% (0.639 vs. 0.572) in mAP. On the VideoAttentionTarget dataset, 15% (0.069 vs. 0.081) in Dist. is achieved. However, the incorporation of the connection map alone contributes significantly less to the average gaze point distance on the GazeFollow dataset and mAP on the VideoAttentionTarget dataset. This discrepancy can be attributed to the VideoAttentionTarget dataset containing a larger number of images than GazeFollow with multiple head-gaze instance annotations, which necessitates improvements in head priors. Overall, integrating head feature re-injection and the connection map in GazeHTA yields superior performance across all evaluation metrics compared to its variants.

Backbones. Although GazeHTA leverages the semantic features extracted from the diffusion model, we expect that integrating the proposed network architecture with alternative backbone models can also yield improvements. To explore the generalizability of our model components, we substitute the backbone with a transformer-based object detector, DETR [4], as also employed in the previous gaze target detection SOTAs [40, 41]. Note the remaining parts of the model including the head feature re-injection and the connection map are unchanged.

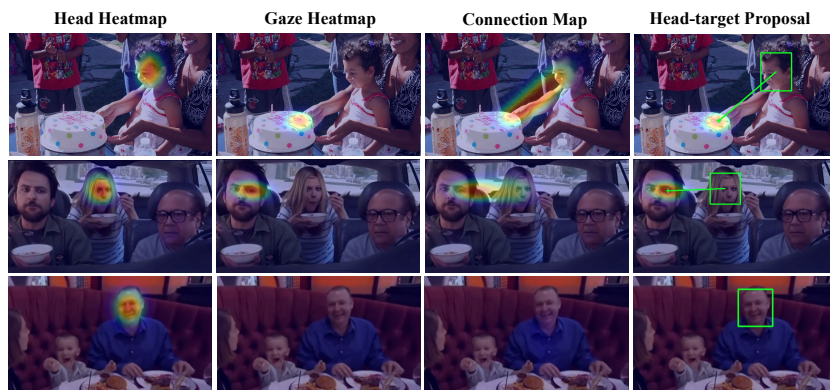


Fig. 3: Predicted head heatmap, gaze heatmap, and the connection map from GazeHTA for the head-target proposal. The first two rows demonstrate the strong associations between heads and in-frame gaze targets established by the connection maps in GazeHTA. These examples show robust prediction of GazeHTA on the head and gaze targets and the connection between them. The third row shows the comprehensive understanding of out-of-frame gaze targets in GazeHTA.

The results of this experiment are presented in the last row of Tab. 3. In comparison to the state-of-the-art methods presented in Tab. 1, our approach with the DETR backbone consistently outperforms across all evaluation metrics. More importantly, since we use the same backbone as in [40, 41], the improvements in performance solely come from the head feature re-injection and the connection map. This demonstrates the ability of the proposed components to generalize beyond a specific backbone.

Compared to GazeHTA that employs Stable Diffusion as the backbone (third row in Tab. 1), using DETR as the backbone achieves inferior performance. It may be attributed to the fact that DETR is trained with a limited number of object classes, whereas Stable Diffusion is trained to generate realistic images, necessitating the learned features to encompass an understanding of diverse objects present in the training data.

4.8 Qualitative Results

In Fig. 3, we provide visualizations for the predicted head-target proposals, featuring their head heatmaps, gaze heatmaps, and connection maps. It is evident that the predicted connection maps establish strong associations between the heads and gaze targets. Notably, in the second row, the connection map effectively links the head and gaze target, even when the person is not facing directly towards the gaze target. In the third row, when the gaze target falls outside the frame, both the gaze heatmap and the connection map show low responses. This observation suggests the comprehensive understanding of gaze targets by GazeHTA in both in-frame and out-of-frame scenarios.

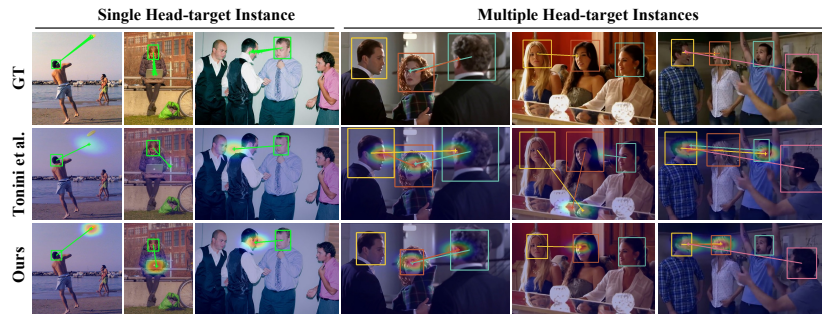


Fig. 4: Qualitative comparison between GazeHTA (bottom) and Tonini et al. [40] (middle) *w.r.t.* the ground-truth (top). We show examples with both single and multiple head-target instance annotations. In the multiple head-target instance examples, different head-target instances are highlighted with distinct colors. Instances where only head bounding boxes are present denote out-of-frame gaze targets. GazeHTA demonstrates superior performance in both single and multiple head-target instance scenarios.

In Fig. 4, we present a visual comparison between Tonini et al. [40] and GazeHTA. We show the detected head bounding boxes alongside their corresponding predicted gaze heatmaps. In the first three columns, Tonini et al. [40] exhibits a limitation in detecting gaze targets when objects are not correctly identified in the object detection stage. In contrast, GazeHTA shows much better results with its fully end-to-end framework and the implicit object understanding inherited from the pre-trained diffusion model. The last two columns are examples of multi-person gaze target detection. Similarly, GazeHTA successfully associates all the head-target instances, while Tonini et al. [40] either fails to identify out-of-frame gaze targets or incorrectly associates head-target instances.

5 Discussion

Conclusion. We present GazeHTA, an end-to-end multi-person gaze target detection framework leveraging semantic features from a pre-trained diffusion model, improving head priors through head feature re-injection, and establishing explicit associations between heads and gaze targets with a connection map. GazeHTA achieves state-of-the-art performance in gaze target detection on two standard datasets.

Limitation and Future Work. Although our experiments have shown the effectiveness of the proposed heatmap-based methodology, we believe that further improvements in head-target modeling could be achieved by formulating the problem to predict a single joint heatmap encompassing information for both heads and gaze targets. Similar to previous approaches, GazeHTA is also constrained by a predefined cap on the number N of head-target instances per image. Future work could explore the feasibility of allowing an arbitrary number of gaze-target instances to better align with real-world scenarios.

References

1. Admoni, H., Scassellati, B.: Social eye gaze in human-robot interaction: a review. *Journal of Human-Robot Interaction* **6**(1), 25–63 (2017) [1](#)
2. Bao, J., Liu, B., Yu, J.: Escnet: Gaze target detection with the understanding of 3d scenes. In: *Proceedings of the IEEE/CVF Conference on Computer Vision and Pattern Recognition*. pp. 14126–14135 (2022) [1](#), [3](#), [9](#), [10](#)
3. Cañigueral, R., Hamilton, A.F.d.C.: The role of eye gaze during natural social interactions in typical and autistic people. *Frontiers in psychology* **10**, 560 (2019) [1](#)
4. Carion, N., Massa, F., Synnaeve, G., Usunier, N., Kirillov, A., Zagoruyko, S.: End-to-end object detection with transformers. In: *European conference on computer vision*. pp. 213–229. Springer (2020) [7](#), [12](#)
5. Chan, E.R., Nagano, K., Chan, M.A., Bergman, A.W., Park, J.J., Levy, A., Aittala, M., De Mello, S., Karras, T., Wetzstein, G.: Generative novel view synthesis with 3d-aware diffusion models (2023) [4](#)
6. Chen, S., Sun, P., Song, Y., Luo, P.: Diffusiondet: Diffusion model for object detection. In: *Proceedings of the IEEE/CVF International Conference on Computer Vision*. pp. 19830–19843 (2023) [2](#), [4](#)
7. Cheng, Y., Lu, F.: Dvgaze: Dual-view gaze estimation. In: *ICCV*. pp. 20632–20641 (2023) [1](#)
8. Chong, E., Ruiz, N., Wang, Y., Zhang, Y., Rozga, A., Rehg, J.M.: Connecting gaze, scene, and attention: Generalized attention estimation via joint modeling of gaze and scene saliency. In: *Proceedings of the European conference on computer vision (ECCV)*. pp. 383–398 (2018) [1](#), [3](#)
9. Chong, E., Wang, Y., Ruiz, N., Rehg, J.M.: Detecting attended visual targets in video. In: *Proceedings of the IEEE/CVF conference on computer vision and pattern recognition*. pp. 5396–5406 (2020) [1](#), [3](#), [8](#), [9](#), [10](#)
10. Clark, K., Jaini, P.: Text-to-image diffusion models are zero shot classifiers. *NeurIPS* **36** (2024) [4](#)
11. Deng, J., Guo, J., Ververas, E., Kotsia, I., Zafeiriou, S.: Retinaface: Single-shot multi-level face localisation in the wild. In: *Proceedings of the IEEE/CVF conference on computer vision and pattern recognition*. pp. 5203–5212 (2020) [6](#), [8](#)
12. Fan, L., Chen, Y., Wei, P., Wang, W., Zhu, S.C.: Inferring shared attention in social scene videos. In: *Proceedings of the IEEE conference on computer vision and pattern recognition*. pp. 6460–6468 (2018) [1](#)
13. Fang, Y., Tang, J., Shen, W., Shen, W., Gu, X., Song, L., Zhai, G.: Dual attention guided gaze target detection in the wild. In: *Proceedings of the IEEE/CVF conference on computer vision and pattern recognition*. pp. 11390–11399 (2021) [2](#), [3](#), [6](#), [9](#), [10](#)
14. Ji, Y., Chen, Z., Xie, E., Hong, L., Liu, X., Liu, Z., Lu, T., Li, Z., Luo, P.: Ddp: Diffusion model for dense visual prediction. *arXiv preprint arXiv:2303.17559* (2023) [2](#), [4](#), [10](#), [11](#)
15. Kuhn, H.W.: The hungarian method for the assignment problem. *Naval research logistics quarterly* **2**(1-2), 83–97 (1955) [7](#)
16. Lian, D., Yu, Z., Gao, S.: Believe it or not, we know what you are looking at! In: *Asian Conference on Computer Vision*. pp. 35–50. Springer (2018) [1](#), [2](#), [3](#), [6](#)
17. Lin, T.Y., Maire, M., Belongie, S., Hays, J., Perona, P., Ramanan, D., Dollár, P., Zitnick, C.L.: Microsoft coco: Common objects in context. In: *Computer Vision–ECCV 2014: 13th European Conference, Zurich, Switzerland, September 6–12, 2014, Proceedings, Part V 13*. pp. 740–755. Springer (2014) [8](#)

18. Loshchilov, I., Hutter, F.: Decoupled weight decay regularization. In: International Conference on Learning Representations (2018) [9](#)
19. Mokady, R., Hertz, A., Bermano, A.H.: Clipcap: Clip prefix for image captioning. arXiv preprint arXiv:2111.09734 (2021) [11](#)
20. Nag, S., Zhu, X., Deng, J., Song, Y.Z., Xiang, T.: Diftad: Temporal action detection with proposal denoising diffusion. arXiv preprint arXiv:2303.14863 (2023) [4](#)
21. Otsu, N.: A threshold selection method from gray-level histograms. IEEE transactions on systems, man, and cybernetics **9**(1), 62–66 (1979) [9](#)
22. Pnvr, K., Singh, B., Ghosh, P., Siddiquie, B., Jacobs, D.: Ld-znet: A latent diffusion approach for text-based image segmentation. In: ICCV. pp. 4157–4168 (2023) [5](#)
23. Ramesh, A., Goyal, S., Chintala, S.: Dall-e: Creating images from text using a conditional transformer. arXiv preprint arXiv:2102.12092 (2021) [4](#)
24. Ramesh, A., Pavlov, M., Goh, G., Gray, S., Voss, C., Radford, A., Chen, M., Sutskever, I.: Zero-shot text-to-image generation. In: International Conference on Machine Learning. pp. 8821–8831. PMLR (2021) [4](#)
25. Recasens, A., Khosla, A., Vondrick, C., Torralba, A.: Where are they looking? Advances in neural information processing systems **28** (2015) [1](#), [3](#), [8](#), [9](#)
26. Recasens, A., Vondrick, C., Khosla, A., Torralba, A.: Following gaze in video. In: Proceedings of the IEEE International Conference on Computer Vision. pp. 1435–1443 (2017) [1](#), [3](#)
27. Rombach, R., Blattmann, A., Lorenz, D., Esser, P., Ommer, B.: High-resolution image synthesis with latent diffusion models. In: Proceedings of the IEEE/CVF conference on computer vision and pattern recognition. pp. 10684–10695 (2022) [2](#), [4](#), [5](#), [9](#), [10](#), [11](#), [12](#)
28. Saharia, C., Chan, W., Saxena, S., Li, L., Whang, J., Denton, E.L., Ghasemipour, K., Gontijo Lopes, R., Karagol Ayan, B., Salimans, T., et al.: Photorealistic text-to-image diffusion models with deep language understanding. Advances in Neural Information Processing Systems **35**, 36479–36494 (2022) [4](#)
29. Saxena, S., Herrmann, C., Hur, J., Kar, A., Norouzi, M., Sun, D., Fleet, D.J.: The surprising effectiveness of diffusion models for optical flow and monocular depth estimation. NeurIPS **36** (2024) [2](#)
30. Schellen, E., Bossi, F., Wykowska, A.: Robot gaze behavior affects honesty in human-robot interaction. Frontiers in Artificial Intelligence **4**, 663190 (2021) [1](#)
31. Shan, W., Liu, Z., Zhang, X., Wang, Z., Han, K., Wang, S., Ma, S., Gao, W.: Diffusion-based 3d human pose estimation with multi-hypothesis aggregation. arXiv preprint arXiv:2303.11579 (2023) [4](#)
32. Sheikhi, S., Odobez, J.M.: Combining dynamic head pose–gaze mapping with the robot conversational state for attention recognition in human–robot interactions. Pattern Recognition Letters **66**, 81–90 (2015) [1](#)
33. Smith, L.N., Topin, N.: Super-convergence: Very fast training of neural networks using large learning rates. In: Artificial intelligence and machine learning for multi-domain operations applications. vol. 11006, pp. 369–386. SPIE (2019) [9](#)
34. Sohl-Dickstein, J., Weiss, E., Maheswaranathan, N., Ganguli, S.: Deep unsupervised learning using nonequilibrium thermodynamics. In: International conference on machine learning. pp. 2256–2265. PMLR (2015) [4](#)
35. Tafasca, S., Gupta, A., Odobez, J.M.: Childplay: A new benchmark for understanding children’s gaze behaviour. In: ICCV. pp. 20935–20946 (2023) [2](#), [3](#), [6](#)
36. Tafasca, S., Gupta, A., Odobez, J.M.: Sharingan: A transformer-based architecture for gaze following. arXiv preprint arXiv:2310.00816 (2023) [3](#)

37. Tang, L., Jia, M., Wang, Q., Phoo, C.P., Hariharan, B.: Emergent correspondence from image diffusion. *NeurIPS* **36** (2024) [4](#)
38. Tomas, H., Reyes, M., Dionido, R., Ty, M., Mirando, J., Casimiro, J., Atienza, R., Guinto, R.: Goo: A dataset for gaze object prediction in retail environments. In: *CVPR*. pp. 3125–3133 (2021) [1](#)
39. Tonini, F., Beyan, C., Ricci, E.: Multimodal across domains gaze target detection. In: *Proceedings of the 2022 International Conference on Multimodal Interaction*. pp. 420–431 (2022) [3](#), [8](#), [9](#)
40. Tonini, F., Dall’Asen, N., Beyan, C., Ricci, E.: Object-aware gaze target detection. In: *Proceedings of the IEEE/CVF International Conference on Computer Vision*. pp. 21860–21869 (2023) [1](#), [2](#), [3](#), [6](#), [7](#), [8](#), [9](#), [10](#), [12](#), [13](#), [14](#)
41. Tu, D., Min, X., Duan, H., Guo, G., Zhai, G., Shen, W.: End-to-end human-gaze-target detection with transformers. In: *2022 IEEE/CVF Conference on Computer Vision and Pattern Recognition (CVPR)*. pp. 2192–2200. *IEEE* (2022) [1](#), [3](#), [6](#), [7](#), [8](#), [9](#), [10](#), [12](#), [13](#)
42. Wang, B., Guo, C., Jin, Y., Xia, H., Liu, N.: Transgop: Transformer-based gaze object prediction. *arXiv preprint arXiv:2402.13578* (2024) [3](#)
43. Yang, L., Kang, B., Huang, Z., Xu, X., Feng, J., Zhao, H.: Depth anything: Unleashing the power of large-scale unlabeled data. *CVPR* (2024) [4](#)
44. Yao, B., Jiang, X., Khosla, A., Lin, A.L., Guibas, L., Fei-Fei, L.: Human action recognition by learning bases of action attributes and parts. In: *2011 International conference on computer vision*. pp. 1331–1338. *IEEE* (2011) [8](#)
45. Yu, Y., Liu, G., Odobez, J.M.: Deep multitask gaze estimation with a constrained landmark-gaze model. In: *Proceedings of the European conference on computer vision (ECCV) workshops*. pp. 0–0 (2018) [1](#)
46. Zhang, X., Sugano, Y., Fritz, M., Bulling, A.: Mpiigaze: Real-world dataset and deep appearance-based gaze estimation. *IEEE TPAMI* **41**(1), 162–175 (2017) [1](#)
47. Zhao, W., Rao, Y., Liu, Z., Liu, B., Zhou, J., Lu, J.: Unleashing text-to-image diffusion models for visual perception. *arXiv preprint arXiv:2303.02153* (2023) [2](#), [4](#), [5](#), [10](#), [11](#), [12](#)